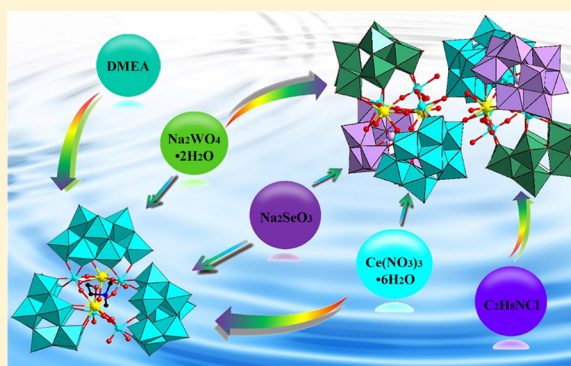


Two Ce³⁺-Substituted Selenotungstates Regulated by *N,N*-Dimethylethanolamine and Dimethylamine Hydrochloride

Hai-Lou Li,^{†,‡} Chen Lian,^{†,‡} Li-Juan Chen,^{*,†} Jun-Wei Zhao,^{*,†} and Guo-Yu Yang^{*,†}[†]Henan Key Laboratory of Polyoxometalate Chemistry, College of Chemistry and Chemical Engineering, Henan University, Kaifeng, Henan 475004, China[‡]MOE Key Laboratory of Cluster Science, School of Chemistry and Chemical Engineering, Beijing Institute of Technology, Beijing 102488, China

Supporting Information

ABSTRACT: Two multi-Ce³⁺-substituted selenotungstates (STs), [HDMEA][H₂N(CH₃)₂]₄H₃Na₄[Ce₂(H₂O)₆(DMEA)W₄O₉(α-SeW₉O₃₃)₃]·26H₂O (**1**) and [H₂N(CH₃)₂]₁₀H₄Na₁₀·[Ce₂W₄O₉(H₂O)₇(α-SeW₉O₃₃)₃]·63H₂O (**2**), were prepared by the one-pot approach of sodium tungstate, sodium selenite, and lanthanide nitrate in an acidic water solution in the presence of *N,N*-dimethylethanolamine (DMEA) or dimethylamine hydrochloride (DMAHC). **1** was obtained in the presence of DMEA, whereas **2** was synthesized in the presence of DMAHC. The trimeric polyoxoanion of **1** contains an unusual V-shaped [Se₃W₂₉O₁₀₃]²⁰⁻ group embracing a prominent heterometal oxide fragment, [Ce₂(H₂O)₆(DMEA)W₂O₅]⁸⁺, and the hexameric polyoxoanion of **2** is constructed from two equivalent trimeric [Ce₂W₄O₉(H₂O)₇(SeW₉O₃₃)₃]²⁴⁻ subunits through two –O–W–O–Ce–O– linkages. The most worthy of attention is that the polyoxoanion of **1** can be approximately viewed as a half of the polyoxoanion of **2** because of the coordination and blocking effect of DMEA. The stability of **1** and **2** in different water pH values was studied by electrospray ionization mass spectroscopy (ESI-MS), and the results manifest that **1** and **2** are stable in pH = 3.5–7.5 and 3.5–7.0, respectively. The oxidation reactions of aromatic sulfides catalyzed by H₂O₂ were studied when **1** or **2** worked as a catalyst, and experimental results reveal that **1** or **2** can serve as available catalysts for the oxidation of aromatic sulfides under mild conditions.



1. INTRODUCTION

Polyoxometalates (POMs) serve as a well-known group of multinuclear metal–oxo compounds and have aroused extensive concern for their alluring architectures and application diversities in molecular catalysis, gas sorption, magnetism, medicine, electronics, and optical devices.^{1–12} In terms of chemical components, POMs are usually assembled by high-oxidation-state early transition metals (TMs), the majority of which are tungsten(VI), molybdenum(VI), vanadium(V), niobium(V), etc.^{13–18} In the aspect of structures, POMs are formed by metal–oxo {MO_n} polyhedra combined via corner/edge/face-sharing modes. Within this field, selenotungstates (STs) as a significant subclass have attracted considerable concern. Great achievements on STs have been made in the past decade. Cronin's reported some unprecedented and intriguing nanoscale poly(ST) aggregates by the one-pot reaction approach in water and explored the assembly rules of some poly(ST) clusters.^{19–23} In 2014, Kalinina et al. discovered a multi-manganese-incorporated dimeric Dawson ST.²⁴ Moreover, Su's group also addressed some innovative STs encapsulating TMs, [(CH₃)₂Sn]²⁺, and lanthanide (Ln) centers and probed the photocatalytic H₂ evolution activity of some species.^{25–28}

It is apparent from the above results that research on ST species is primarily focused on pure STs and TM-containing STs (TMCSTs), and less work is involved in Ln-containing STs (LCSTs); therefore, the continuous synthesis and discovery of novel LCSTs with desirable properties is still a challenging research field. In the past several years, our laboratory has invested substantial effort in preparing neoteric LCSTs by the one-pot approach of sodium tungstate, lanthanide nitrate, sodium selenite, and organic solubilizers and obtained some particular LCSTs.^{29–31} As a part of our continuous exploration on LCSTs based on the one-pot reaction approach, *N,N*-dimethylethanolamine (DMEA) or dimethylamine hydrochloride (DMAHC) was introduced to our reaction system because they can facilitate enhancement of the solubility of Ln cations in the Se–O–W system. It can be prudentially found from our previous results that dimethylamine components from DMAHC are often protonated and work as organocations to stabilize the desired LCSTs. However, DMEA not only consists of an amino group that can be protonated to act as a counteranion but also consists of

Received: February 27, 2019

Published: June 17, 2019

an alcoholic group that can coordinate to the metal centers; therefore, the utilization of DMEA may result in the structure discrepancies of some desired LCSTs. Under the guidance of these considerations, we performed exploration on the Ce–Se–W–O system in the presence of DMEA or DMAHC. In the present paper, we obtained two neoteric multi-Ce³⁺-substituted STs, [HDMEA][H₂N(CH₃)₂]₄H₃Na₄[Ce₂(H₂O)₆(DMEA)W₄O₉(α-SeW₉O₃₃)₃]₂·26H₂O (**1**) and [H₂N(CH₃)₂]₁₀H₄Na₁₀[Ce₂W₄O₉(H₂O)₇(α-SeW₉O₃₃)₃]₂·63H₂O (**2**) (Table S1). It is fairly interesting that the structure difference of **1** and **2** mainly stems from the utilization of DMEA or DMAHC because of the fact that **1** was prepared in the presence of DMEA while **2** was prepared in the presence of DMAHC. The most worthy of attention is that the polyoxoanion of **1** can be approximately viewed as a half of the polyoxoanion of **2** because of the coordination and blocking effect of DMEA. The stability of **1** and **2** in water under different pH values was investigated by virtue of electrospray ionization mass spectroscopy (ESI-MS), indicating that **1** and **2** are stable in pH = 3.5–7.5 and 3.5–7.0, respectively. Furthermore, the effects of **1** and **2** as catalysts on the oxidation reactions of aromatic sulfides by H₂O₂ were evaluated. Catalytic oxidation experimental results reveal the good catalytic performances of **1** and **2** as catalysts toward the oxidation of aromatic sulfides by H₂O₂.

2. EXPERIMENTAL SECTION

Preparation of [HDMEA][H₂N(CH₃)₂]₄H₃Na₄[Ce₂(H₂O)₆(DMEA)W₄O₉(α-SeW₉O₃₃)₃]₂·26H₂O (1**).** With stirring, Na₂WO₄·2H₂O (4.000 g, 12.127 mmol) and Na₂SeO₃ (0.200 g, 1.156 mmol) were put in 40 mL of water, to which DMEA (2 mL, 1 mol·L⁻¹) was added. The pH of the solution was set at 3.0 by the addition of HCl (6 mol·L⁻¹) dropwise. Subsequently, Ce(NO₃)₃·6H₂O (0.300 g, 0.691 mmol) was added to the solution, and the pH was readjusted to 3.0. Finally, the solution was filtered after stirring for 30 min. The filtrate was left to evaporate at room temperature, and yellow block crystals of **1** formed after 4 weeks. Yield: 0.54 g (17.40%) based on Ce(NO₃)₃·6H₂O. Elem anal. Calcd for **1**: C, 2.14; H, 1.37; N, 0.94; W, 63.47; Ce, 3.12; Se, 2.64; Na, 1.02. Found: C, 2.41; H, 1.55; N, 0.86; W, 63.55; Ce, 3.32; Se, 2.74; Na, 1.10. IR (cm⁻¹): 3402, 3128, 2772, 1628, 1464, 968, 892, 856, 790 (Figure S3).

Preparation of [H₂N(CH₃)₂]₁₀H₄Na₁₀[Ce₂W₄O₉(H₂O)₇(SeW₉O₃₃)₃]₂·63H₂O (2**).** The synthetic process of **2** is similar to that of **1** with DMAHC (2.002 g, 24.552 mmol) in place of DMEA. Yellow block crystals for **2** formed after 3 weeks. Yield: 0.67 g (21.58%) based on Ce(NO₃)₃·6H₂O. Elem anal. Calcd for **2**: C, 1.34; H, 1.33; N, 0.78; W, 63.42; Ce, 3.12; Se, 2.64; Na, 1.28. Found: C, 1.53; H, 1.60; N, 0.89; W, 64.15; Ce, 3.67; Se, 2.79; Na, 1.34. IR (cm⁻¹): 3415, 3147, 2792, 1632, 1471, 969, 889, 851, 795 (Figure S3).

3. RESULTS AND DISCUSSION

Synthetic Discussion. Over the past 10 years, some pure STs, TMCSTs, and organotin-incorporated STs were reported; nevertheless, little interest has been paid to multinuclear LCSTs because there are some obstacles in the design and preparation of neoteric multinuclear LCSTs. The difficulties mainly lie in three aspects: First, in comparison with arsenotungstates and tungstoantimonates, no available ST precursors can be used as building blocks to make multinuclear LCSTs. Second, highly oxyphilic Ln cations were directly reacted with in situ formed ST fragments, which usually resulted in amorphous precipitates rather than crystals. Third, according to our experiments, it can be found that the solubility of lanthanide nitrate in the in situ formed ST reaction system is not good without the participation of

organic components, which renders the preparation of multinuclear LCSTs to be uneasy. To cope with the first difficulty, we utilized the one-pot reaction approach of commercial materials such as sodium tungstate, lanthanide nitrate, and sodium selenite in an acidic water solution. To solve the second and third difficulties, we introduced organic components such as DMEA or DMAHC in the reaction to improve the solubility of Ln ions; moreover, these organic components can be protonated in an acidic environment and function as larger counteranions to promote crystallization of target compounds and increase the stability of target compounds. Thus, **1** and **2** were triumphantly made. Parallel experimental results revealed that **1** and **2** were easily formed in pH = 2.5–3.3. The pH of 3.0 led to the highest yield. Besides, the effect of organic solubilizing agents on the structures of products was taken into account. When there was no DMEA or DMAHC in the reaction, the system was cloudy and abundant amorphous precipitations appeared, resulting in the preparation failure of **1** and **2**. On the contrary, when DMEA or DMAHC was used, the solution is clear in the stirring procedure, **1** and **2** were successfully obtained. **1** was obtained in the existence of DMEA, while **2** was made in the presence of DMAHC. In addition, when DMEA and DMAHC were simultaneously utilized, only the trimer **1** was obtained and no hexamer **2** was found.

Structure Description. The good phase purity of **1** and **2** was confirmed via powder X-ray diffraction patterns (Figure S1). The structure unit of **1** comprises a unique organic–inorganic hybrid trimeric entity of [Ce₂(H₂O)₆(DMEA)W₄O₉(α-SeW₉O₃₃)₃]¹²⁻ (**1a**; Figures 1a and S2a), 3 protons, 1 [HDMEA]⁺, 4 [H₂N(CH₃)₂]⁺, 4 Na⁺ ions, and 26 crystal water molecules. Notably, [H₂N(CH₃)₂]⁺ cations may be due to the degradation of DMEA because dimethylamine was used as a raw material in the preparation of DMEA. The bond valences of 6+, 4+, and 3+ for W, Se, and Ce atoms in **1** can be

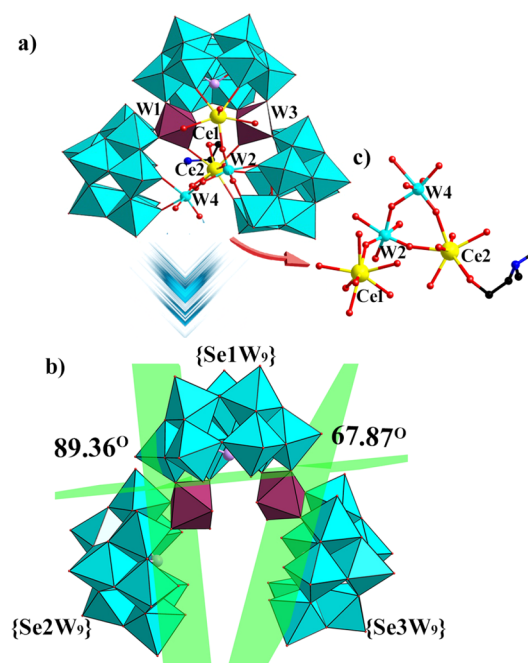


Figure 1. (a) View of **1a**. (b) V-shaped [Se₃W₉O₁₀₃]²⁰⁻ cluster in **1a**. (c) Tetranuclear heterometal [Ce₂(H₂O)₆(DMEA)W₂O₅]¹⁸⁺ cluster in **1a**.

calculated by bond valence sum (Table S2).³² The bond valences of O53 and O87 atoms connected to W2 and W4 atoms are 0.407 and 0.315, which indicate that O53 and O87 are aqua ligands. The infrastructure of **1a** could be described as one tetranuclear heterometal $[\text{Ce}_2(\text{H}_2\text{O})_6(\text{DMEA})\text{W}_2\text{O}_5]^{8+}$ cluster (Figure 1c) encapsulated by a V-shaped $[\text{Se}_3\text{W}_{29}\text{O}_{103}]^{20-}$ cluster (Figure 1b). The unprecedented $[\text{Se}_3\text{W}_{29}\text{O}_{103}]^{20-}$ cluster is constructed from three $[\text{SeW}_9\text{O}_{33}]^{8-}$ units linked by two $\{\text{WO}_6\}$ (W3 and W1) octahedra. The $[\text{Se}_3\text{W}_{29}\text{O}_{103}]^{20-}$ cluster can also be imagined as a fusion of two $[\text{Se}_2\text{W}_{19}\text{O}_{68}]^{14-}$ units by sharing a trivacant Keggin $[\alpha\text{-SeW}_9\text{O}_{33}]^{8-}$ fragment; as far as we know, such a configuration is quite rare. Although two $[\text{Se}_2\text{W}_{19}\text{O}_{68}]^{14-}$ units in the $[\text{Se}_3\text{W}_{29}\text{O}_{103}]^{20-}$ cluster are very similar, there is a conspicuous difference between them: the intersection angle (89.36°) formed by $[\alpha\text{-Se1W}_9\text{O}_{33}]^{8-}$ and $[\alpha\text{-Se2W}_9\text{O}_{33}]^{8-}$ in $[\text{Se1Se2W}_{19}\text{O}_{68}]^{14-}$ is larger than that (67.87°) formed by $[\alpha\text{-Se1W}_9\text{O}_{33}]^{8-}$ and $[\alpha\text{-Se3W}_9\text{O}_{33}]^{8-}$ in $[\text{Se1Se3W}_{19}\text{O}_{67}(\text{H}_2\text{O})]^{14-}$, which may be mainly ascribed to the fact that 3 W and 2 Ce centers are nipped in the pocket position of $[\text{Se1Se2W}_{19}\text{O}_{68}]^{14-}$, whereas 2 W and 2 Ce centers are embedded in the vacancy of $[\text{Se1Se3W}_{19}\text{O}_{68}]^{14-}$. In **1a**, the V-shaped $[\text{Se}_3\text{W}_{29}\text{O}_{103}]^{20-}$ cluster embraces the tetranuclear heterometal $[\text{Ce}_2(\text{H}_2\text{O})_6(\text{DMEA})\text{W}_2\text{O}_5]^{8+}$ cluster through 12 $\mu_2\text{-O}$ atoms. In the tetranuclear heterometal $[\text{Ce}_2(\text{H}_2\text{O})_6(\text{DMEA})\text{W}_2\text{O}_5]^{8+}$ cluster, the W2 atom joins the $[\alpha\text{-Se3W}_9\text{O}_{33}]^{8-}$ segment via 2 $\mu_2\text{-O}$ atoms, 2 Ce^{3+} (Ce1 and Ce2) ions via 2 $\mu_2\text{-O}$ atoms, and the W4 atom through 1 $\mu_2\text{-O}$ atom and a terminal O atom, and the W2–O distances range from 1.747(11) to 2.250(14) Å. The W4 atom is combined with the $[\alpha\text{-Se2W}_9\text{O}_{33}]^{8-}$ segment via 2 $\mu_2\text{-O}$ atoms, 1 Ce^{3+} ion via 1 $\mu_2\text{-O}$ atom, the W2 atom through 1 $\mu_2\text{-O}$ atom and two terminal O atoms, and the W4–O distances are between 1.723(13) and 2.344(13) Å. Both Ce1^{3+} and Ce2^{3+} ions exhibit distorted square-antiprismatic geometry, and the Ce–O distances vary in the range of 2.408(12)–2.651(13) Å. The coordination sphere of the Ce1^{3+} ion is defined by 2 $\mu_2\text{-O}$ atoms from 1 $[\alpha\text{-SeW}_9\text{O}_{33}]^{8-}$ unit, 3 $\mu_2\text{-O}$ atoms from 3 $\{\text{WO}_6\}$ (W1, W2, and W3) groups, and 3 aqua ligands. Differently, the coordination sphere of the Ce2^{3+} ion is constituted by 2 $\mu_2\text{-O}$ atoms from one $[\alpha\text{-Se3W}_9\text{O}_{33}]^{8-}$ unit, 4 $\mu_2\text{-O}$ atoms from 4 different $\{\text{WO}_6\}$ (W1, W2, W3, and W4) groups, 1 aqua ligand, and 1 $\mu_2\text{-O}$ atom from DMEA.

Alternatively, **1a** (Figure 2a) can be perceived as an unprecedented hexanuclear heterometal $[\text{Ce}_2(\text{H}_2\text{O})_6(\text{DMEA})\text{W}_4\text{O}_9]^{12+}$ cluster (Figure 2b) linking three $[\alpha\text{-SeW}_9\text{O}_{33}]^{8-}$ fragments (Figure 2c) in the triangular distribution motif by 16 $\mu_2\text{-O}$ atoms from 3 $[\alpha\text{-SeW}_9\text{O}_{33}]^{8-}$ fragments. Interestingly, the hexanuclear heterometal $[\text{Ce}_2(\text{H}_2\text{O})_6(\text{DMEA})\text{W}_4\text{O}_9]^{12+}$ cluster shows a trigonal bipyramid defined by 3 W (W1, W2, and W3) atoms situated at the basal plane and 2 Ce (Ce1 and Ce2) atoms occupying two vertexes, and the W4 atom connects W2 and Ce2 atoms through 2 $\mu_2\text{-O}$ atoms (Figure 2d).

It should be pointed out that **1a** somewhat resembles the $[\{\text{Y}(\text{B-}\alpha\text{-SbW}_9\text{O}_{31})(\text{OH})_2)(\text{CH}_3\text{COO})(\text{H}_2\text{O})\}_3(\text{WO}_4)]^{17-}$ (**3**) cluster (Figure 2e) reported by Kortz et al. in 2011.³³ Although **1a** and **3** display the same rare-earth-substituted triangular polyoxoanion skeletons, but significant discrepancies can be found among them: (a) The trivacant Keggin POM fragments are different; **1a** contains the $[\alpha\text{-SeW}_9\text{O}_{33}]^{8-}$ fragment (Figure 2c), while **3** includes the $[\alpha\text{-SbW}_9\text{O}_{33}]^{9-}$ fragment (Figure 2g). (b) The connection modes are distinct;

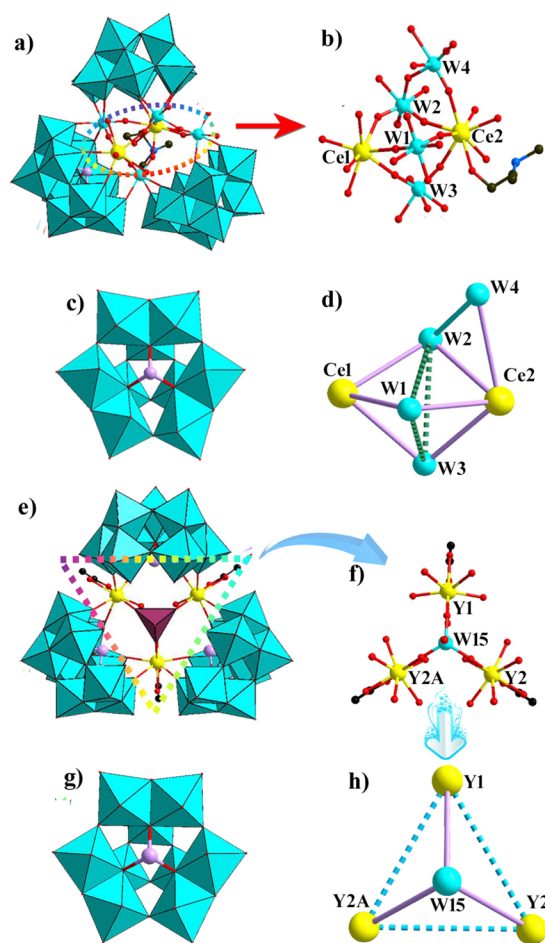


Figure 2. (a) View of **1a**. (b) Hexanuclear heterometal $[\text{Ce}_2(\text{H}_2\text{O})_6(\text{DMEA})\text{W}_4\text{O}_9]^{12+}$ cluster in **1a**. (c) $[\alpha\text{-SeW}_9\text{O}_{33}]^{8-}$ fragment in **1a**. (d) Simplified geometry of the $[\text{Ce}_2(\text{H}_2\text{O})_6(\text{DMEA})\text{W}_4\text{O}_9]^{12+}$ cluster. (e) Polyoxoanion of **3**. (f) Tetranuclear heterometal $[\text{Y}_3(\text{H}_2\text{O})_3(\text{CH}_3\text{COO})_3(\text{WO}_4)]^{4+}$ cluster in **3**. (g) $[\alpha\text{-SbW}_9\text{O}_{33}]^{9-}$ fragment in **3**. (h) Simplified geometry of $[\text{Y}_3(\text{H}_2\text{O})_3(\text{CH}_3\text{COO})_3(\text{WO}_4)]^{4+}$ cluster. Symmetry code: A, $x, 0.5 - y, z$.

3 trivacant Keggin POM fragments in **1a** are bridged by a hexanuclear heterometal $[\text{Ce}_2(\text{H}_2\text{O})_6(\text{DMEA})\text{W}_4\text{O}_9]^{12+}$ cluster through W–O–W and Ce–O–W linkers, whereas 3 trivacant Keggin POM fragments in **3** are directly joined together by a tetranuclear heterometal $[\text{Y}_3(\text{CH}_3\text{COO})_3(\text{H}_2\text{O})_3(\text{WO}_4)]^{4+}$ cluster through Y–O–W linkers (Figure 2f). (c) The coordination environment of W atoms is different in the hexanuclear heterometal $[\text{Ce}_2(\text{H}_2\text{O})_6(\text{DMEA})\text{W}_4\text{O}_9]^{12+}$ cluster and the tetranuclear heterometal $[\text{Y}_3(\text{CH}_3\text{COO})_3(\text{H}_2\text{O})_3(\text{WO}_4)]^{4+}$ cluster. (d) The arrangement fashions of metal centers in the hexanuclear $\{\text{Ce}_2\text{W}_4\}$ cluster in **1a** and the tetranuclear $\{\text{Y}_3\text{W}\}$ cluster in **3** are distinguishing: in the hexanuclear $\{\text{Ce}_2\text{W}_4\}$ of **1**, three equatorial sites of the trigonal bipyramid are occupied by 3 W centers, while two polar sites are occupied by 2 Ce centers and 1 W center links to one edge formed by a W center and a Ce center via double $\mu_2\text{-oxo}$ bridges (Figure 2d), whereas the Basal plane of the trigonal pyramid in **3** is constituted by 3 Y centers and the apical site is occupied by 1 W center (Figure 2h). (e) Coordination modes of organic ligands are diverse: in **1**, a DMEA ligand coordinates to the Ce^{3+} ion by the alcohol O atom in the end-on mode; in contrast, each of 3 acetate ligands

in **3** chelates with a Y^{3+} ion by carboxylic O atoms in the bidentate mode.

Under the same synthetic conditions as those of **1**, in which DMEA was replaced by DMAHC, unexpectedly, the hexameric LCST **2** was obtained. The structural unit of **2** comprises 1 hexameric $[Ce_2W_4O_9(H_2O)_7(SeW_9O_{33})_3]^{24-}$ (**2a**) polyoxoanion (Figure 3a,b), 4 protons, 10 $[H_2N(CH_3)_2]^+$ ions, 10 Na^+

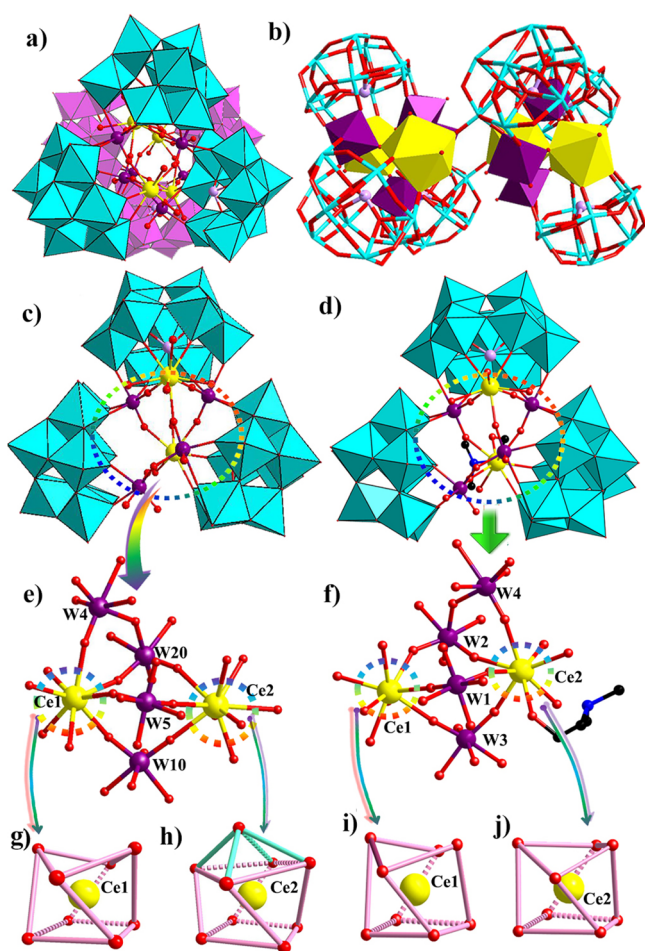


Figure 3. (a and b) Representations of **2a** viewed along different directions. (c) Trimeric $[Ce_2W_4O_9(H_2O)_7(SeW_9O_{33})_3]^{12-}$ cluster in **2a**. (d) Trimeric **1a**. (e) Hexanuclear heterometal $[Ce_2W_4O_9(H_2O)_7]^{12+}$ cluster in **2a**. (f) Hexanuclear heterometal $[Ce_2(H_2O)_6(DMEA)W_4O_9]^{12+}$ cluster of **1a**. (g and h) Coordination geometry of $Ce1^{3+}$ and $Ce2^{3+}$ ions in **2a**. (i and j) Coordination geometry of $Ce1^{3+}$ and $Ce2^{3+}$ ions in **1a**.

ions, and 63 crystal water molecules. The bond valences for W, Se, and Ce atoms are calculated as 6+, 4+, and 3+, respectively (Table S3).³² In addition, the bond valences of O56 and O60 atoms connected to W20 and W4 atoms are 0.450 and 0.351, which indicate that O56 and O60 are aqua molecules. The hexameric **2a** polyoxoanion is formed by two trimeric entities $[Ce_2W_4O_9(H_2O)_7(SeW_9O_{33})_3]^{12-}$ connected by double Ce–O–W linkers. The trimeric entity of **2a** (Figures 3c and S2b) is constructed from a fascinating hexanuclear heterometal $[Ce_2W_4O_9(H_2O)_7]^{12+}$ cluster (Figure 3e) in the center joining 3 trivalent Keggin $[\alpha-SeW_9O_{33}]^{8-}$ fragments via 16 μ_2 -O atoms from 3 $[\alpha-SeW_9O_{33}]^{8-}$ fragments. The trimeric entity of **2a** is very similar to the trimeric **1a** (Figure 3d). When the structures of **2a** and **1a** are compared, it can be clearly seen

that **1a** can be approximately viewed as a half of **2a** because of the coordination and blocking effect of DMEA. It should be noted that the hexanuclear heterometal $[Ce_2W_4O_9(H_2O)_7]^{12+}$ cluster in **2a** rather resembles the hexanuclear heterometal $[Ce_2(H_2O)_6(DMEA)W_4O_9]^{12+}$ cluster (Figure 3f) in **1a**. Notably, albeit their structures are very analogous, **1a** is still somewhat disparate from **2a**: (a) The prominent divergence is that **1a** contains a DMEA ligand and its alcoholic hydroxyl O atom coordinating to the $Ce2^{3+}$ ion. (b) Their other distinction is that $Ce1^{3+}$ and $Ce2^{3+}$ ions in **2a** inhabit in an eight/nine-coordinate square-antiprism/monocapped square antiprism (Figure 3g,h), whereas $Ce1^{3+}$ and $Ce2^{3+}$ ions of **1a** adopt an eight-coordinate square antiprism (Figure 3i,j). Alternatively, the hexameric **2a** can be perceived as two vacant Keggin $[SeW_{10}O_{36}(H_2O)]^{8-}$ fragments acting as bridges connecting two sandwich-type $[(W_3Ce_2(H_2O)_7O_6)(SeW_9O_{33})_2]^{4-}$ subunits (Figure 4a–d). The alignment mode of two sandwich-type $[(W_3Ce_2(H_2O)_7O_6)(SeW_9O_{33})_2]^{4-}$ moieties in **2a** (Figure 4c) takes after that of two sandwich-type $[(W_3Eu_2(H_2O)_8AsO_8(OH))(B-\alpha-AsW_9O_{33})_2]^{8-}$ (**4a**) moieties in $[(W_3Eu_2(H_2O)_8AsO_8(OH))(B-\alpha-AsW_9O_{33})_2]^{16-}$ (**4**) (Figure 4e).³⁴ It is easy to find that the sandwich-type $[(W_3Ce_2(H_2O)_7O_6)(SeW_9O_{33})_2]^{4-}$ moiety (Figure 4d) in **2a** is also similar to the sandwich-type **4a** subunit (Figure 4f) in **4**. The similarities between them are as follows: (a) Both sandwich-type subunits are assembled from two trilacunary POM segments sandwiching one pentanuclear $\{W_3Ln_2\}$ cluster (Figure 4d–f); in addition, the distances between two trilacunary POM segments are similar, 7.557 Å for $[(W_3Ce_2(H_2O)_7O_6)(SeW_9O_{33})_2]^{4-}$ in **2a** and 7.564 Å for **4a** in **4**. (b) The pentanuclear $\{W_3Ln_2\}$ clusters in **2a** and **4** illustrate similar trigonal-bipyramidal distribution fashions. (c) The polyoxoanions of **2a** and **4** contain four Ln atoms. Nevertheless, there still exist some differences between them: (a) The bridging fragments to connect two sandwich-type subunits together are distinct; namely, the divacant Keggin $[SeW_{10}O_{36}(H_2O)]^{8-}$ fragment serves as the bridging fragment in **2**, while the triangular pyramidal $\{AsO_2(OH)\}$ works as the bridging fragment in **4**; in addition, the distances between two sandwich-type subunits are discrepant, 13.746 Å for **2** and 12.584 Å for **4**. (b) The connection modes of the bridging fragments linking two sandwich-type subunits are different. In **2a**, the vacant Keggin $[SeW_{10}O_{36}(H_2O)]^{8-}$ fragment joins 1 sandwich-type subunit through 3 O–W–O and 1 O–Ce–O–W–O linkers and the other through 1 O–Ce–O–W–O linker. In **4**, the $\{AsO_2(OH)\}$ group as a μ_2 -bridge connects 2 sandwich-type fragments through the W–O–As–O–W linker.

Solution Behavior. As is well-known, POMs are hyper-sensitive to the pH of the medium. The ESI-MS technique can be applied to measure the stability and integrity of POMs in aqueous solution.^{35–45} Hence, the ESI-MS spectra of **1** and **2** dissolved in different pH water solutions were measured (Figures S5 and S6). The pH of the water solution was regulated using dilute sodium hydroxide and sulfuric acid. After **1** or **2** was dissolved in water, the pH was 5.0. In the ESI-MS spectrum of **1** collected in pH = 5.0 water, the strong peak at m/z 1353.5743 is derived from the typical molecular fragment $[(C_2H_8N)H_5Ce_2(H_2O)_7W_4O_9(SeW_9O_{33})_3]^{6-}$, which indicates that the polyoxoanion of **1** maintains a good integrity in water. It can be explicitly seen from Figure S5 that the peak at m/z 1353.5743 intensity is almost unchanged when the pH gradually decreases to about 3.0. Upon further lowering of the pH, this peak disappears, which implies that the polyoxoanion

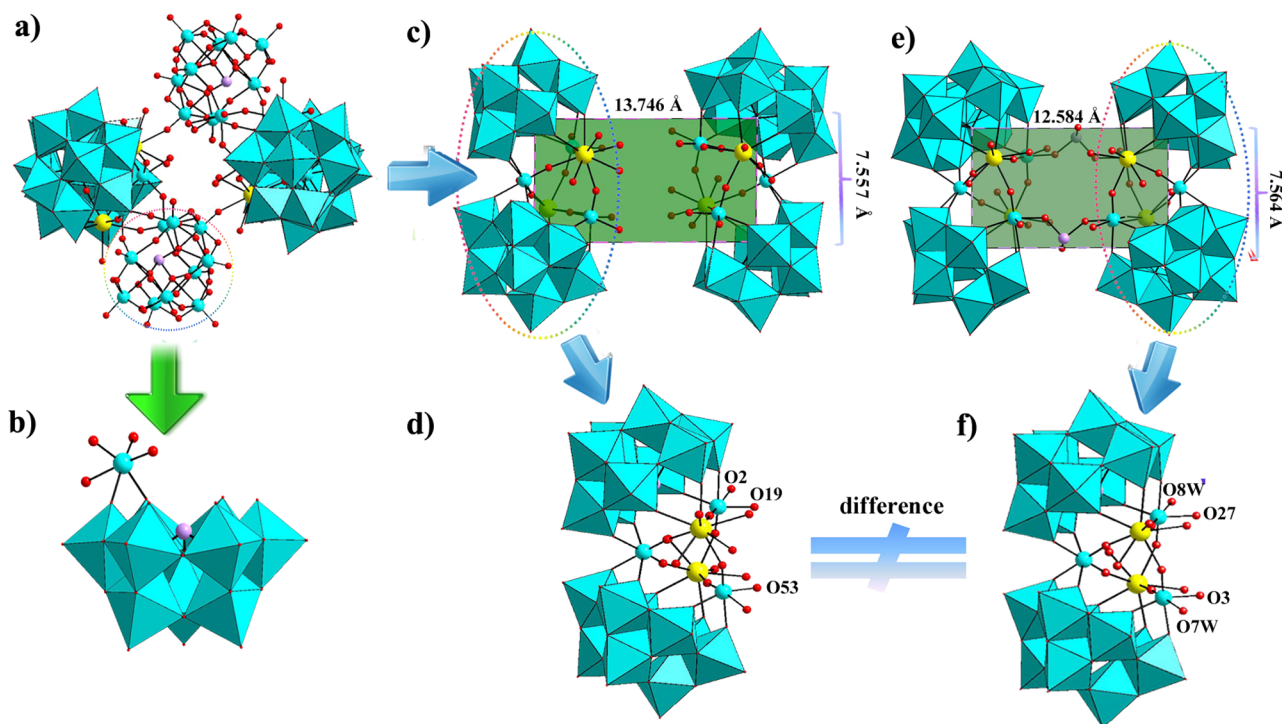


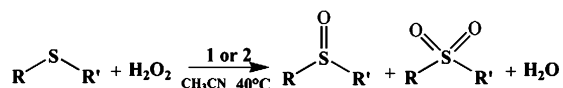
Figure 4. (a) View of **2a**. (b) Vacant Keggin $[(\text{SeW}_{10}\text{O}_{36}(\text{H}_2\text{O}))]^{8-}$ fragment in **2a**. (c) Alignment mode of two sandwich-type $[(\text{W}_3\text{Ce}_2(\text{H}_2\text{O})_7\text{O}_6)(\text{SeW}_9\text{O}_{33})_2]^{4-}$ moieties in **2a**. (d) Sandwich-type $[(\text{W}_3\text{Ce}_2(\text{H}_2\text{O})_7\text{O}_6)(\text{SeW}_9\text{O}_{33})_2]^{4-}$ moiety in **2**. (e) $[(\text{W}_3\text{Eu}_2(\text{H}_2\text{O})_8\text{AsO}_8(\text{OH}))(\text{B-}\alpha\text{-AsW}_9\text{O}_{33})_2]^{16-}$ polyoxoanion of **4**. (f) Sandwich-type moiety of **4a**.

skeleton was destroyed. When the pH varies from 5.0 to 7.5, the peak at m/z 1353.5743 can be clearly observed. When the pH is higher than 7.5, this peak almost completely disappears, suggesting that the polyoxoanion skeleton has been decomposed. The above results indicate that the polyoxoanion skeleton of **1** in water can be stable between pH = 3.5 and 7.5. Similarly, as indicated in Figure S6, the polyoxoanion skeleton of **2** in water can be stable between pH = 3.5 and 7.0. In addition, the stability of **1** and **2** in pH = 5 and 6 water solutions at different times was also tested by ESI-MS experiments, revealing that the polyoxoanion skeleton of **1** or **2** is still stable at least until 6 h (Figures S7–S10).

Catalytic Properties. Sulfones and sulfoxides have a wide range of applications in biology, medicine, fine chemicals, etc.,^{46,47} so the efficient conversion, precise selectivity, and mild reaction conditions of thioethers are critical. POMs as catalysts in the process of catalytic oxidation of organic species have high active sites and excellent stability.^{48,49}

It has been reported that POMs can effectively catalyze the oxidation of aromatic sulfides in the presence of H_2O_2 .⁵⁰ Herein, **1** and **2** served as catalysts to investigate the oxygenation reactions of aromatic sulfides at 40 °C with a green oxidant H_2O_2 (Scheme 1). The oxygenation products of aromatic sulfides were determined by the gas chromatography (GC)–mass spectrometry (MS) technique. The selectivity and conversion were quantified by the GC technique [such as

Scheme 1. Catalytic Oxidation of Aromatic Sulfides



diphenyl sulfide (DPS), (4-methoxyphenyl)methyl sulfide, (4-nitrophenyl)methyl sulfide, etc.; Figures S11–S13].

First, we explored the conversion and selectivity of catalytic oxidation of **1** and **2** as catalysts for DPS by comparison with $\text{Na}_2\text{WO}_4 \cdot 2\text{H}_2\text{O}$, $\text{Ce}(\text{NO}_3)_3 \cdot 6\text{H}_2\text{O}$, and $\text{Na}_2\text{WO}_4 \cdot 2\text{H}_2\text{O} + \text{Ce}(\text{NO}_3)_3 \cdot 6\text{H}_2\text{O}$ as catalysts as well as without any catalyst, respectively. Obviously, in the absence of catalyst, the conversion of DPS is only 8%, and extremely small amount of diphenyl sulfone (DPSO_2) is obtained. Additionally, the comparison results of different catalysts are illustrated in Figure 5; it is easy to find that **1** and **2** as catalysts have extremely high

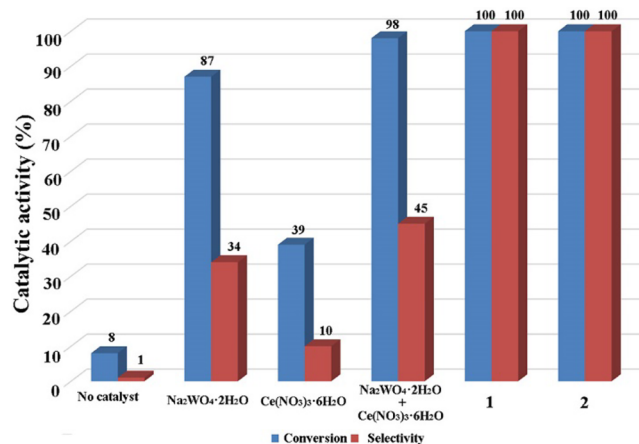
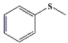
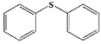
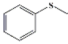
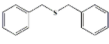
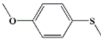
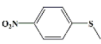
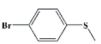
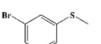
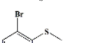
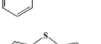
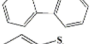


Figure 5. Effect of different catalysts on the conversion of DPS and the selectivity of DPSO_2 . Reaction conditions: 0.5 mmol of substrate, O/S (oxidant/substrate) = 3, S/C (substrate/catalyst) = 500, 3 mL of CH_3CN .

conversion and selectivity. Therefore, **1** and **2** may serve as excellent catalysts in the aromatic thioether oxidation reaction.

Besides, under the same reaction conditions, as shown in Table 1, we also conducted a series of catalytic oxidation

Table 1. Summary of Catalytic Oxidation of Different Aromatic Sulfides Using 1 as a Catalyst.^a

Entry	Substrate	Time. (h)	Temp. (°C)	Cov. (%)	RR'SO/R'RSO ₂	Selectivity (%)
1		1	40	100	0	100
2		1	40	100	0	100
3		1	40	100	0	100
4		1	40	100	0	100
5		1	40	98	0	100
6		1	40	100	0	100
7		1	40	100	0	100
8		1	40	100	0	100
9		1	40	100	0	100
10		1	40	100	0	100
11		1	40	99	0	100

^aReaction conditions: substrate = 0.5×10^{-3} mol, O/S = 3, S/C = 500, CH₃CN (3 mL).

experiments on 10 other aromatic thioethers in the presence of **1**. Gratifyingly, these aromatic thioethers almost completely disappear in the catalytic oxidation experiments (>98% conversion), and the products are all sulfones (100% selectivity). Especially, 2-bromothiobenzene, benzothiofuran, and dibenzothiofuran, for which catalyzing oxidation is generally extremely difficult, also have satisfactory catalytic results in the presence of **1**. This is an unexpected result of those catalytic thioether experiments in the presence of polyoxotungstates. For example, recently, Niu et al. reported a ruthenium-substituted arsenotungstate as a catalyst under optimal experimental conditions, which only has 52% and 69% for the catalytic oxidation conversion of benzothiofuran and dibenzothiofuran, respectively.⁵¹

Moreover, under optimal reaction conditions, the recycling tests of catalyst **1** were carried out when DPS was used as the substrate. As shown in Figure 6, the catalytic activity of **1** is not attenuated after five-cycle experiments (>99 conversion and 100% selectivity), which demonstrates that the catalytic performance of **1** is very stable. Furthermore, the stability of the catalyst was confirmed by IR spectra (Figure S14a). The results reveal that **1** does not undergo structural change after the catalytic reaction.

Similarly, we also conducted catalytic oxidation experiments on 10 other aromatic thioethers in the presence of **2**. As shown in Table 2, the catalytic performance of **2** is also extremely excellent. In 2014, our group reported a gigantic hexameric Zr₂₄-cluster-substituted polytungstate and investigated a series of thioether oxidation catalyses.⁵² Although it is also a hexamer, its catalytic performance is lower than that of **2**

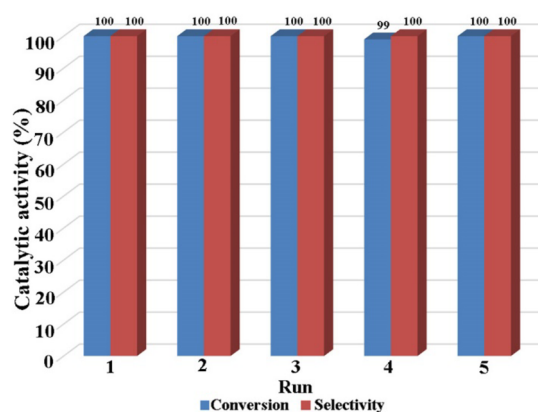
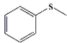
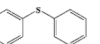
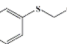
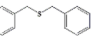
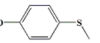
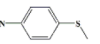
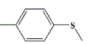
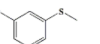
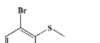
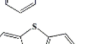
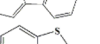


Figure 6. Recycling test results of catalyst **1** upon DPS as the substrate.

Table 2. Summary of Catalytic Oxidation of Different Aromatic Sulfides Using 2 as a Catalyst.^a

Entry	Substrate	Time. (h)	Temp. (°C)	Cov. ^[a] (%)	Selectivity (%) ^[a]
1		1	40	100	100
2		1	40	100	100
3		1	40	100	100
4		1	40	100	100
5		1	40	99	100
6		1	40	100	100
7		1	40	100	100
8		1	40	100	100
9		1	40	100	100
10		1	40	100	100
11		1	40	98	100

^aThe reaction conditions are similar to those in Table 1.

under optimal conditions, especially in the catalytic oxidation of 2-bromothiobenzene and dibenzothiofuran. In the presence of the Zr₂₄-cluster-substituted polytungstate, the catalytic oxidation result of 2-bromothiobenzene is not very ideal (69% conversion and 10% selectivity) and there is almost no reaction for dibenzothiofuran. In addition, the optimal experimental temperature of the Zr₂₄-cluster-substituted polytungstate is higher than that of this experiment, and the amount of catalyst is more than **2**.

In addition, we also investigated the recycling tests and structural stability of catalyst **2** by recycling the catalytic oxidation of DPS. As shown in Figure 7, in the cycle experiments, the conversion of DPS is higher than 99% and the selectivity of DPSO₂ is 100%. Additionally, no obvious discrepancy was observed in IR spectra before and after the catalyst experiments (Figure S14b).

The catalytic oxidation mechanism of aromatic sulfides is similar to those in refs 53–56. First, the oxidant H₂O₂ interacts with the terminal bonds (W=O) in the ST skeletons of **1** or **2**

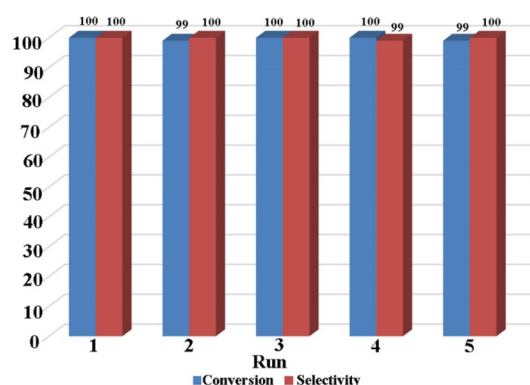


Figure 7. Recycling test results of catalyst 2 with DPS as the substrate.

to form active POM peroxides. Subsequently, the peroxide species transfer the O atoms to aromatic sulfides, and the initial terminal bonds are regenerated and can be used to restart the catalytic cycle.

4. CONCLUSIONS

In brief, two multi-Ce³⁺-substituted STs 1 and 2 were triumphantly manufactured through the one-pot reaction approach in an acidic water medium. Interestingly, the trimeric Ce³⁺-substituted ST 1 was formed in the presence of DMAHC, while the hexameric Ce³⁺-substituted ST 2 was obtained when DMAHC was replaced by DMEA. Noteworthy, the trimeric polyoxoanion of 1 contains an unusual V-shaped [Se₃W₂₉O₁₀₃]²⁰⁻ group embracing an outstanding heterometal [Ce₂(H₂O)₆(DMEA)W₂O₅]⁸⁺ fragment, whereas the hexameric polyoxoanion of 2 is constructed from two equivalent trimeric [Ce₂W₄O₉(H₂O)₇(SeW₉O₃₃)₃]₂²⁴⁻ subunits via two -O-W-O-Ce-O- linkers, which are rather rare in LCSTs. Above all, the oxidation reactions of aromatic sulfides catalyzed by H₂O₂ were evaluated when 1 or 2 worked as a catalyst, and the results exhibit that 1 or 2 can serve as the available catalyst for the oxidation of aromatic sulfides under mild conditions. Furthermore, 1 and 2 exhibit good stability in recycling experiments. This work not only provides us with a good reaction strategy for controlling the structure diversity of multi-Ln-substituted POMs but also expands the application potentials of LCSTs in the field of the oxygenation reactions of thioethers. In the future, we will design many more multi-Ln-substituted POM materials by changing the types of organic solubilizers and then explore their catalytic properties in organic reaction systems.

■ ASSOCIATED CONTENT

Supporting Information

The Supporting Information is available free of charge on the ACS Publications website at DOI: 10.1021/acs.inorgchem.9b00582.

Bond valences of some atoms, relevant figures, IR and ESI-MS spectra, and TG curves (PDF)

Accession Codes

CCDC 1870260 and 1870289 contain the supplementary crystallographic data for this paper. These data can be obtained free of charge via www.ccdc.cam.ac.uk/data_request/cif, or by emailing data_request@ccdc.cam.ac.uk, or by contacting The Cambridge Crystallographic Data Centre, 12 Union Road, Cambridge CB2 1EZ, UK; fax: +44 1223 336033.

■ AUTHOR INFORMATION

Corresponding Authors

*E-mail: ljchen@henu.edu.cn.

*E-mail: zhaojunwei@henu.edu.cn.

*E-mail: ygy@bit.edu.cn.

ORCID

Jun-Wei Zhao: 0000-0002-7685-1309

Guo-Yu Yang: 0000-0002-0911-2805

Notes

The authors declare no competing financial interest.

■ ACKNOWLEDGMENTS

This work was supported by the Natural Science Foundation of China (Grants 21771052, 21671054, 21571048, and 21871077) and the 2014 Special Foundation for Scientific Research Project of Henan University (Project XXJC20140001).

■ REFERENCES

- (1) Marrot, J.; Pilette, M. A.; Haouas, M.; Floquet, S.; Taulelle, F.; López, X.; Poblet, J. M.; Cadot, E. Polyoxometalates paneling through {Mo₂O₂S₂} coordination: cation-directed conformations and chemistry of a supramolecular hexameric scaffold. *J. Am. Chem. Soc.* **2012**, *134*, 1724–1737.
- (2) Zhao, Y.; Deng, D. S.; Ma, L. F.; Ji, B. M.; Wang, L. Y. A new copper-based metal–organic framework as a promising heterogeneous catalyst for chemo- and regio-selective enamination of β-ketoesters. *Chem. Commun.* **2013**, *49*, 10299–10301.
- (3) Heine, J.; Müller-Buschbaum, K. Engineering metal-based luminescence in coordination polymers and metal–organic frameworks. *Chem. Soc. Rev.* **2013**, *42*, 9232–9242.
- (4) Descalzo, A. B.; Martínez-Mañez, R.; Sancenón, F.; Hoffmann, K.; Rurack, K. The supramolecular chemistry of organic–inorganic hybrid materials. *Angew. Chem., Int. Ed.* **2006**, *45*, 5924–5948.
- (5) Zheng, S. T.; Zhang, J.; Li, X. X.; Fang, W. H.; Yang, G. Y. Cubic polyoxometalate–organic molecular cage. *J. Am. Chem. Soc.* **2010**, *132*, 15102–15103.
- (6) Artetxe, B.; Reinoso, S.; San Felices, L.; Lezama, L.; Gutiérrez-Zorrilla, J. M.; García, J. A.; Galán-Mascarós, J. R.; Haider, A.; Kortz, U.; Vicent, C. Cation-directed dimeric versus tetrameric assemblies of lanthanide-stabilized dilacunary Keggin tungstogermanates. *Chem. - Eur. J.* **2014**, *20*, 12144–12156.
- (7) Zhao, J. W.; Li, H. L.; Ma, X.; Xie, Z. G.; Chen, L. J.; Zhu, Y. S. Lanthanide-connecting and lone-electron-pair active trigonal-pyramidal-AsO₃ inducing nanosized poly(polyoxotungstate) aggregates and their anticancer activities. *Sci. Rep.* **2016**, *6*, 26406.
- (8) Ma, P. T.; Hu, F.; Wang, J. P.; Niu, J. Y. Carboxylate covalently modified polyoxometalates: From synthesis, structural diversity to applications. *Coord. Chem. Rev.* **2019**, *378*, 281–309.
- (9) Li, H. L.; Liu, Y. J.; Liu, J. L.; Chen, L. J.; Zhao, J. W.; Yang, G. Y. Structural Transformation from Dimerization to Tetramerization of Serine-decorated rare-earth-incorporated arsenotungstates induced by the usage of rare-earth salts. *Chem. - Eur. J.* **2017**, *23*, 2673–2689.
- (10) Wang, Y.-J.; Zhou, Y.-Y.; Hao, H.-G.; Song, M.; Zhang, N.; Yao, S.; Yan, J.-H.; Zhang, Z.-M.; Lu, T.-B. Capped polyoxometalate pillars between metal–organic layers for transferring a supramolecular structure into a covalent 3D framework. *Inorg. Chem.* **2018**, *57*, 1342–1349.
- (11) Lin, H.; Wang, J.-W.; Guo, X.-W.; Yao, S.; Liu, M.; Zhang, Z.-M.; Lu, T.-B. Phosphorized polyoxometalate-etched ironhydroxide porous nanotubes for efficient electrocatalytic oxygen evolution. *J. Mater. Chem. A* **2018**, *6*, 24479–24485.
- (12) Rajnák, C.; Titiš, J.; Moncol, J.; Mičová, R.; Boča, R. Field-induced slow magnetic relaxation in a mononuclear manganese(II) complex. *Inorg. Chem.* **2019**, *58*, 991–994.

- (13) Pope, M. T. *Heteropoly and Isopoly Oxometalates*; Springer: Berlin, 1983.
- (14) Müller, A.; Peters, F.; Pope, M. T.; Gatteschi, D. Polyoxometalates: very large clusters nanoscale magnets. *Chem. Rev.* **1998**, *98*, 239–272.
- (15) Long, D. L.; Burkholder, E.; Cronin, L. Polyoxometalate clusters, nanostructures and materials: from self assembly to designer materials and devices. *Chem. Soc. Rev.* **2007**, *36*, 105–121.
- (16) Kortz, U.; Müller, A.; van Slageren, J.; Schnack, J.; Dalal, N. S.; Dressel, M. Polyoxometalates: fascinating structures, unique magnetic properties. *Coord. Chem. Rev.* **2009**, *253*, 2315–2327.
- (17) Cronin, L.; Müller, A. From serendipity to design of polyoxometalates at the nanoscale, aesthetic beauty and applications. *Chem. Soc. Rev.* **2012**, *41*, 7333–7334.
- (18) Zheng, S. T.; Yang, G. Y. Recent advances in paramagnetic-TM-substituted polyoxometalates (TM = Mn, Fe, Co, Ni, Cu). *Chem. Soc. Rev.* **2012**, *41*, 7623–7646.
- (19) Yan, J.; Long, D. L.; Cronin, L. Development of a building block strategy to access gigantic nanoscale heteropolyoxotungstates by using SeO_3^{2-} as a template linker. *Angew. Chem., Int. Ed.* **2010**, *49*, 4117–4120.
- (20) Yan, J.; Gao, J.; Long, D. L.; Miras, H. N.; Cronin, L. Self-assembly of a nanosized, saddle-shaped, solution-stable polyoxometalate anion built from pentagonal building blocks: $[\text{H}_{34}\text{W}_{119}\text{Se}_8\text{Fe}_2\text{O}_{420}]^{54-}$. *J. Am. Chem. Soc.* **2010**, *132*, 11410–11411.
- (21) Gao, J.; Yan, J.; Beeg, S.; Long, D. L.; Cronin, L. One-pot versus sequential reactions in the self-assembly of gigantic nanoscale polyoxotungstates. *J. Am. Chem. Soc.* **2013**, *135*, 1796–1805.
- (22) Cameron, J. M.; Gao, J.; Long, D. L.; Cronin, L. Self-assembly and structural transformations of high-nuclearity palladium-rich polyoxometalates. *Inorg. Chem. Front.* **2014**, *1*, 178–185.
- (23) Cameron, J. M.; Gao, J.; Vilà-Nadal, L.; Long, D. L.; Cronin, L. Formation, self-assembly and transformation of a transient selenotungstate building block into clusters, chains and macrocycles. *Chem. Commun.* **2014**, *50*, 2155–2157.
- (24) Kalinina, I. V.; Peresypkina, E. V.; Izarova, N. V.; Nkala, F. M.; Kortz, U.; Kompankov, N. B.; Moroz, N. K.; Sokolov, M. N. Cyclic tungstoselenites based on $\{\text{Se}_2\text{W}_{12}\}$ units. *Inorg. Chem.* **2014**, *53*, 2076–2082.
- (25) Chen, W. C.; Li, H. L.; Wang, X. L.; Shao, K. Z.; Su, Z. M.; Wang, E. B. Assembly of cerium (III)-stabilized polyoxotungstate nanoclusters with $\text{SeO}_3^{2-}/\text{TeO}_3^{2-}$ templates: from single polyoxoanions to inorganic hollow spheres in dilute solution. *Chem. - Eur. J.* **2013**, *19*, 11007–11015.
- (26) Chen, W. C.; Qin, C.; Wang, X. L.; Li, Y. G.; Zang, H. Y.; Jiao, Y. Q.; Huang, P.; Shao, K. Z.; Su, Z. M.; Wang, E. B. Assembly of Fe-substituted Dawson-type nanoscale selenotungstate clusters with photocatalytic H_2 evolution activity. *Chem. Commun.* **2014**, *50*, 13265–13267.
- (27) Chen, W. C.; Qin, C.; Li, Y. G.; Zang, H. Y.; Shao, K. Z.; Su, Z. M.; Wang, E. B.; Liu, H. S. Assembly of tetrameric dimethyltin-functionalized selenotungstates: from nanoclusters to one-dimensional chains. *Chem. Commun.* **2015**, *51*, 2433–2436.
- (28) Chen, W. C.; Qin, C.; Wang, X. L.; Wu, C. X.; Li, Y. G.; Zang, H. Y.; Shao, K. Z.; Su, Z. M.; Wang, E. B. Trimeric hexa-dimethyltin-functionalized selenotungstate $[\{\text{Sn}(\text{CH}_3)_2(\text{CH}_3\text{COO})\}_3\{\text{Sn}(\text{CH}_3)_2\}_3\{\text{Se}_2\text{W}_{18}\text{O}_{62}(\text{OH})(\text{H}_2\text{O})\}_3]^{18-}$. *CrystEngComm* **2016**, *18*, 2820–2824.
- (29) Li, H. L.; Yang, W.; Chai, Y.; Chen, L. J.; Zhao, J. W. A novel Dawson-like cerium(IV)-hybridizing selenotungstate $\text{Na}_{13}\text{H}_7[\text{Ce}(\text{SeW}_{17}\text{O}_{59})_2] \cdot 31\text{H}_2\text{O}$. *Inorg. Chem. Commun.* **2015**, *56*, 35–40.
- (30) Li, H. L.; Liu, Y. J.; Li, Y. M.; Chen, L. J.; Zhao, J. W.; Yang, G. Y. Unprecedented selenium and lanthanide simultaneously bridging selenotungstate aggregates stabilized by four tetra-vacant Dawson-like $\{\text{Se}_2\text{W}_{14}\}$ units. *Chem. - Asian J.* **2018**, *13*, 2897–2907.
- (31) Liu, Y. J.; Li, H. L.; Lu, C. T.; Gong, P. J.; Ma, X. Y.; Chen, L. J.; Zhao, J. W. Organocounterions-assisted and pH-controlled self-assembly of five nanoscale high-nuclear lanthanide substituted heteropolytungstates. *Cryst. Growth Des.* **2017**, *17*, 3917–3928.
- (32) Brown, I. D.; Altermatt, D. Bond-valence parameters obtained from a systematic analysis of the inorganic crystal structure database. *Acta Crystallogr., Sect. B: Struct. Sci.* **1985**, *B41*, 244–247.
- (33) Ibrahim, M.; Mal, S. S.; Bassil, B. S.; Banerjee, A.; Kortz, U. Yttrium (III)-containing tungstoantimonate (III) stabilized by tetrahedral WO_4^{2-} capping unit, $[\{\text{Y}(\alpha\text{-SbW}_6\text{O}_{31}(\text{OH})_2)(\text{CH}_3\text{COO})(\text{H}_2\text{O})\}_3(\text{WO}_4)]^{17-}$. *Inorg. Chem.* **2011**, *50*, 956–960.
- (34) Li, H. L.; Liu, Y. J.; Zheng, R.; Chen, L. J.; Zhao, J. W.; Yang, G. Y. Trigonal pyramidal $\{\text{AsO}_2(\text{OH})\}$ bridging tetranuclear rare-earth encapsulated polyoxotungstate aggregates. *Inorg. Chem.* **2016**, *55*, 3881–3893.
- (35) Miras, H. N.; Wilson, E. F.; Cronin, L. Unravelling the complexities of inorganic and supramolecular self-assembly in solution with electrospray and cryospray mass spectrometry. *Chem. Commun.* **2009**, 1297–1311.
- (36) Tsunashima, R.; Long, D. L.; Miras, H. N.; Gabb, D.; Pradeep, C. P.; Cronin, L. The construction of high-nuclearity isopolyoxoniobates with pentagonal building blocks: $[\text{HNb}_{27}\text{O}_{76}]^{16-}$ and $[\text{H}_{10}\text{Nb}_{31}\text{O}_{93}(\text{CO}_3)]^{23-}$. *Angew. Chem., Int. Ed.* **2010**, *49*, 113–116.
- (37) Zheng, Q.; Vilà-Nadal, L.; Lang, Z. L.; Chen, J.-J.; Long, D.-L.; Mathieson, J. S.; Poblet, J. M.; Cronin, L. Self-sorting of heteroanions in the assembly of cross-shaped polyoxometalate clusters. *J. Am. Chem. Soc.* **2018**, *140*, 2595–2601.
- (38) Sokolov, M. N.; Adonin, S. A.; Sinkevich, P. L.; Vicent, C.; Mainichev, D. A.; Fedin, V. P. Organometallic derivatives of Rh- and Ir-substituted polyoxotungstates with Keggin structure: reactivity screening by electrospray ionization mass-spectrometry. *Dalton Trans.* **2012**, *41*, 9889–9892.
- (39) Li, F.; Long, D.-L.; Cameron, J. M.; Miras, H. N.; Pradeep, C. P.; Xu, L.; Cronin, L. Cation induced structural transformation and mass spectrometric observation of the missing dodecavanadomanganate(IV). *Dalton Trans.* **2012**, *41*, 9859–9862.
- (40) Sokolov, M. N.; Adonin, S. A.; Sinkevich, P. L.; Vicent, C.; Mainichev, D. A.; Fedin, V. P. Keggin-type polyoxometalates $[\text{PW}_{11}\text{O}_{39}\text{MCl}]^{5-}$ with noble metals (M = Rh and Ir): novel synthetic entries and ESI-MS directed reactivity screening. *Z. Anorg. Allg. Chem.* **2014**, *640*, 122–127.
- (41) Miras, H. N.; Wilson, E. F.; Cronin, L. Unravelling the complexities of inorganic and supramolecular self-assembly in solution with electrospray and cryospray mass spectrometry. *Chem. Commun.* **2009**, 1297–1311.
- (42) Sokolov, M. N.; Adonin, S. A.; Mainichev, D. A.; Vicent, C.; Zakharchuk, N. F.; Danilenko, A. M.; Fedin, V. P. Synthesis and characterization of $[\text{PW}_{11}\text{O}_{39}\text{Ir}(\text{H}_2\text{O})]^{4-}$: successful incorporation of Ir into polyoxometalate framework and study of the substitutional lability at the Ir(III) site. *Chem. Commun.* **2011**, *47*, 7833–7835.
- (43) Vicent, C.; Adonin, S. A.; Anyushin, A. V.; Mainichev, D. A.; Sokolov, M. Gas-phase fragmentation reactions of Keggin-type $\{\text{PW}_{11}\text{O}_{39}\text{M}\}$ (M = Rh, Ir, and Ru) polyoxometalates as fingerprints of the ligands attached at the noble metal site. *Eur. J. Inorg. Chem.* **2014**, *2014*, 5618–5624.
- (44) Bonchio, M.; Bortolini, O.; Conte, V.; Sartorel, A. Electrospray behavior of lacunary Keggin-type polyoxotungstates $[\text{XW}_{11}\text{O}_{39}]^p$ (X Si, P): mass spectrometric evidence for a concentration dependent incorporation of an MO_n (M = W^{VI} , Mo^{VI} , V^{V}) unit into the polyoxometalate vacancy. *Eur. J. Inorg. Chem.* **2003**, *2003*, 699–704.
- (45) Bray, T. H.; Copping, R.; Shuh, D. K.; Gibson, J. K. Electrospray ionization mass spectrometry of a cerium (III) phosphomolybdate complex: condensed and gas-phase cluster chemistry. *Int. J. Mass Spectrom.* **2011**, *299*, 35–46.
- (46) Carreno, M. C. Applications of sulfoxides to asymmetric synthesis of biologically active compounds. *Chem. Rev.* **1995**, *95*, 1717–1760.
- (47) Sheldon, R.; Arends, I. W. C.; Dijkstra, A. New developments in catalytic alcohol oxidations for fine chemicals synthesis. *Catal. Today* **2000**, *57*, 157–166.
- (48) Wang, S. S.; Yang, G. Y. Recent advances in polyoxometalate-catalyzed reactions. *Chem. Rev.* **2015**, *115*, 4893–4962.

(49) Li, H.-L.; Lian, C.; Yin, D.-P.; Jia, Z.-Y.; Yang, G.-Y. A new hepta-nuclear Ti-oxo-cluster-substituted tungstoantimonate and its catalytic oxidation of thioethers. *Cryst. Growth Des.* **2019**, *19*, 376–380.

(50) Kholdeeva, O. A.; Maksimov, G. M.; Maksimovskaya, R. I.; Kovaleva, L. A.; Fedotov, M. A.; Grigoriev, V. A.; Hill, C. L. A dimeric titanium-containing polyoxometalate. Synthesis, characterization, and catalysis of H₂O₂-based thioether oxidation. *Inorg. Chem.* **2000**, *39*, 3828–3837.

(51) Han, M. D.; Niu, Y. J.; Wan, R.; Xu, Q. F.; Lu, J. K.; Ma, P. T.; Zhang, C.; Niu, J. Y.; Wang, J. P. A crown-shaped Ru-substituted arsenotungstate for selective oxidation of sulfides with hydrogen peroxide. *Chem. - Eur. J.* **2018**, *24*, 11059–11066.

(52) Huang, L.; Wang, S. S.; Zhao, J. W.; Cheng, L.; Yang, G. Y. Synergistic combination of multi-Zr^{IV} cations and lacunary Keggin germanotungstates leading to a gigantic Zr₂₄-cluster-substituted polyoxometalate. *J. Am. Chem. Soc.* **2014**, *136*, 7637–7642.

(53) Ribeiro, S.; Granadeiro, C. M.; Silva, P.; Almeida Paz, F. A.; de Biani, F. F.; Cunha-Silva, L.; Balula, S. S. An efficient oxidative desulfurization process using terbium-polyoxometalate@MIL-101(Cr). *Catal. Sci. Technol.* **2013**, *3*, 2404–2414.

(54) Niu, Y. J.; Xu, Q. F.; Wang, Y.; Li, Z.; Lu, J. K.; Ma, P. T.; Zhang, C.; Niu, J. Y.; Wang, J. P. Preparation, characterization, and catalytic performances of a pyrazine dicarboxylate-bridging rare-earth-containing polytungstoarsenate aggregate for selective oxidation of thiophenes and deep desulfurization of model fuels. *Dalton Trans.* **2018**, *47*, 9677–9684.

(55) Nisar, A.; Lu, Y.; Zhuang, J.; Wang, X. Polyoxometalate nanocone nanoreactors: magnetic manipulation and enhanced catalytic performance. *Angew. Chem.* **2011**, *123*, 3245–3250.

(56) Li, H.; Jiang, X.; Zhu, W.; Lu, J.; Shu, H.; Yan, Y. Deep oxidative desulfurization of fuel oils catalyzed by decatungstates in the ionic liquid of [Bmim]PF₆. *Ind. Eng. Chem. Res.* **2009**, *48*, 9034–9039.